10-1-2002

H2O–D2O Condensation in A Supersonic Nozzle

Christopher H. Heath
Worcester Polytechnic Institute

Kiril A. Streletzky
Cleveland State University, K.STRELETZKY@csuohio.edu

Barbara E. Wyslouzil
Worcester Polytechnic Institute, barbaraw@wpi.edu

Judith Woelk
University of Cologne

Reinhard Strey
University of Cologne

Publisher's Statement

H_2O–D_2O condensation in a supersonic nozzle

Christopher H. Heath, Kiril Streletzky, and Barbara E. WyslouzilJudith Wölk and Reinhard Strey

Citation: **117**, 6176 (2002); doi: 10.1063/1.1502644
View online: http://dx.doi.org/10.1063/1.1502644
View Table of Contents: http://aip.scitation.org/toc/jcp/117/13
Published by the American Institute of Physics

H_2O-D_2O condensation in a supersonic nozzle

Christopher H. Heath, Kiril Streletzky, and Barbara E. Wyslouzil[a)]
Department of Chemical Engineering, Worcester Polytechnic Institute, Worcester, Massachusetts 01609-2280

Judith Wölk and Reinhard Strey
Institut für Physikalische Chemie, Universität zu Köln, 50939 Köln, Germany

(Received 18 April 2002; accepted 2 July 2002)

We examined the condensation of H_2O, D_2O, and four intermediate mixtures (20, 40, 60, and 80 mol % D_2O) in a supersonic nozzle. Because the physical and chemical properties of protonated and deuterated water are so similar, this system is ideal for studying the change in condensation behavior as a function of condensible composition. In our experiments dilute mixtures of condensible vapor in N_2 are expanded from three different stagnation temperatures resulting in a broad range of onset temperatures (190–238 K) and pressures (27–787 kPa). For a fixed stagnation temperature, the partial pressure required to maintain the onset of condensation at a given location or temperature in the nozzle is consistently higher for H_2O than for D_2O. In contrast, the supersaturation at fixed onset temperature is usually higher for D_2O than for H_2O and this difference increases toward lower temperature. The partial pressure at onset for the intermediate mixtures varied linearly between the values observed for the pure components in this ideal system. © *2002 American Institute of Physics.* [DOI: 10.1063/1.1502644]

I. INTRODUCTION

Water condensation occurs in many natural and industrial processes including cloud formation, power generation, and turbomechanical flows. One way to enhance our understanding of the behavior of this important substance is to conduct experiments using light water, H_2O, heavy water, D_2O, and their mixtures. The H_2O-D_2O system is also ideal for studying binary condensation because the molecules are so similar. Pure H_2O and D_2O have comparable equilibrium vapor pressures, and the other important physical properties, in particular surface tension, do not differ greatly. Thus, unlike binary condensation in aqueous alcohol systems,[1–3] surface enrichment effects should not be important.

Condensation studies in nozzles began indirectly with the development of high speed wind tunnels, where researchers found that heat addition from condensing water vapor altered the desired expansions.[4] Thus, early nozzle condensation experiments focused primarily on water. Water often played a role in condensation experiments of other substances because the air used as a carrier gas frequently contained trace amounts of moisture.[5,6] In nozzles, water condensation experiments range from those that start with pure steam[7,8] to those where the water is highly diluted in an inert carrier gas.[2,9] The current experiments are in the latter category with a maximum water concentration of 3.5 mol % water or 0.017 kg_{H_2O}/kg_{N_2}. In addition to the onset measurements made in nozzles, water nucleation rates have been measured extensively using expansion cloud chambers,[10–14] shock tubes,[15,16] and the diffusion cloud chamber.[17]

In contrast to H_2O there is only a limited data base available for the condensation of D_2O. The earliest work is that of Flood and Tronstad[18] who measured the critical supersaturations for D_2O condensation in an expansion cloud chamber in 1935. In 1977 Lee reported the condensation onset pressures and temperatures for both H_2O and D_2O in a shock tube.[19] Given the scatter in his data, it is difficult to distinguish an effect due to deuteration. The most comprehensive nucleation rate measurements to date for D_2O are those of Wölk and Strey.[14] In an extensive set of nucleation pulse chamber experiments, they measured nucleation rates J for H_2O and D_2O in the range $10^6 < J/\mathrm{cm}^{-3}\ \mathrm{s}^{-1} < 10^9$ for temperatures between 220 and 260 K. They found that for a given condensible vapor pressure and temperature the nucleation rates of D_2O were higher than those for H_2O, but that the data agreed within experimental error if the rates were compared at the same supersaturation and temperature. Our experiments complement the work of Wölk and Strey because peak nucleation rates in conventional nozzle experiments are about 8 orders of magnitude higher and onset temperatures are up to 30 K lower than those in the nucleation pulse chamber.

Finally, this work is also motivated by our ongoing small angle neutron scattering (SANS) experiments from aerosols. Nucleation in supersonic nozzles produces a high number density aerosol ($\sim 10^{12}\ \mathrm{cm}^{-3}$) of nanometer-size droplets.[20–23] The small droplet size makes it difficult to uniquely characterize the aerosol size distribution using conventional optical techniques, and sampling the aerosol is difficult because the droplets evaporate as soon as the flow decelerates. When the droplets consist of molecules with a high neutron scattering length density, such as D_2O, then SANS experiments can quantitatively determine the properties of the aerosol.[20,21,24] Although the two isotopic forms of water have similar physical properties, the presence or absence of

a)Author to whom correspondence should be addressed; electronic mail: barbaraw@wpi.edu

an additional neutron in the nucleus of the hydrogen atom substantially changes the nuclear properties of the compound. Thus, light water aerosols produced in our nozzle have too weak a neutron scattering signal for aerosol–SANS experiments to give useful results. Studying the change in condensation phenomena as a function of mixture composition should make it possible to better account for effects of deuteration and therefore learn about the behavior of weakly scattering molecules by studying their strongly scattering counterparts.

Here we describe the results of our conventional H_2O-D_2O condensation studies starting from a stagnation pressure p_0 of 59.6 kPa and stagnation temperatures T_0 of 13.5, 26.0, and 35.0 °C. We report the onset data and discuss the general nature of the condensation processes for pure H_2O and D_2O, and mixtures containing 20, 40, 60, and 80 mol % D_2O. In addition to providing a basis for planning the SANS experiments,[22,23] this extensive data base is an invaluable resource for modeling unary and multicomponent droplet formation under extremes of temperature and supersaturation.

The paper is organized as follows. We first discuss minor changes made to the system before and during the H_2O-D_2O condensation experiments. We then present and discuss the experimental results in the order that they were generated. Finally, we summarize the work and present our conclusions.

II. EXPERIMENT

Detailed descriptions of the experimental setup, procedures, and data reduction methods are available in a previous paper.[2] Here, we briefly summarize the experimental technique and describe minor changes made to the system.

In our apparatus, a mixture of noncondensible gas and condensible vapor expands through a supersonic nozzle cooling at rates of up to $\sim 10^6$ K/s. Supersaturations as high as several hundred are reached in the nozzle before the vapor condenses *via* homogeneous nucleation and droplet growth. All experiments start at a fixed stagnation pressure and temperature, and the static pressure is measured along the length of the nozzle using a narrow diameter probe. Expansion of a pure carrier gas characterizes the area ratio of the nozzle. To determine the thermodynamic state of the flow in the presence of condensation, we integrate the diabatic flow equations using the measured area ratio and the condensing flow pressure profile as input.[2] A 0.5 K difference between the temperature of the condensing flow and the temperature for an isentropic expansion of the same gas mixture defines the onset of condensation.

In these binary condensation experiments we fix the $H_2O:D_2O$ ratio in the gas phase, and then vary the partial pressure of the condensible vapor in the expanding gas to determine the relationship between onset pressure and temperature (the Wilson line). We then change the $H_2O:D_2O$ ratio and repeat the experiments to explore the effect of gas phase composition on the onset of condensation in this highly ideal system.

A. Equipment changes

All condensation experiments are performed from constant plenum pressure. The stagnation pressure p_0 differs slightly from the plenum pressure, however, because of several nonisentropic losses incurred between the plenum and the entrance to the nozzle. In the setup used for the H_2O-*n*-alcohol experiments,[2] the greatest pressure drop was due to a mesh screen located between the flow straightener and the nozzle that supported the leading edge of the pressure probe. For these experiments, we replaced the mesh by four wires forming a diagonal cross pattern and reduced the pressure losses from 1.2 to 0.47 kPa. The remaining pressure losses come from abrupt changes in the cross-sectional flow area at the entrance and exit of the flow straightener, and to the presence of a 1.6 mm diam resistance temperature device (RTD probe) that vertically divides the flow. A second change was to decrease the diameter of the static pressure probe d_{probe} from 1.65 to 1.27 mm to minimize its effect on the flowfield. This change reduced the area of the throat obstructed by the probe from 3.4% to 2.0%. For the SANS experiments,[22,23] the pressure probe is removed from the nozzle and, thus, using a smaller probe makes the pressure trace and SANS experiments more consistent. The diameter of the holes d_{hole} in the side of the static pressure probe were also changed to maintain the ratio $d_{\text{hole}}/d_{\text{probe}} \leqslant 1/3$ required for accurate measurement.[25]

For the experiments starting from $T_0 = 13.5$ and 35.0 °C, the nozzle sidewalls containing the Si windows were replaced. On one side, a clear polycarbonate wall let us confirm that both the static pressure and stagnation pressure probes sampled the flow in a stable manner. On the other side, an Al sidewall with three pressure taps let us ensure that static pressure measurements taken with the centerline probes were correct.

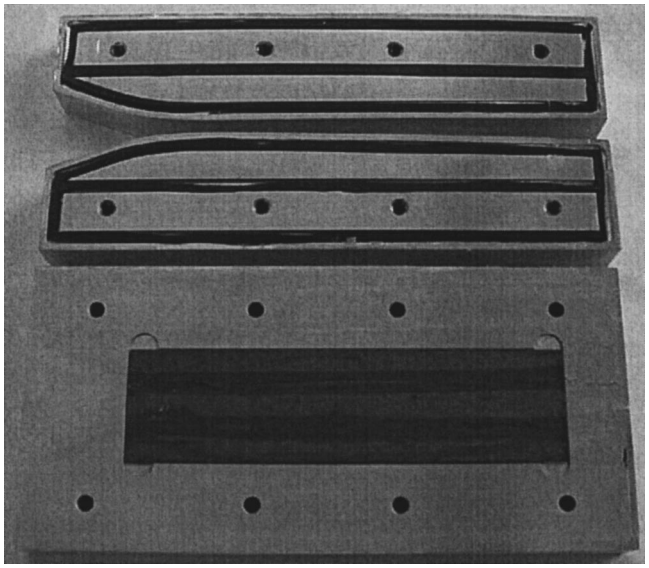

FIG. 1. (Top.) The two-dimensional Laval nozzle (nozzle A), has a total opening angle of 1.77°, and is displayed for flow from left to right. The central o-ring minimizes leakage between the bolt holes and the flow channel. (Bottom) The single crystal Si windows in the sidewalls are required for the small angle neutron scattering experiments.

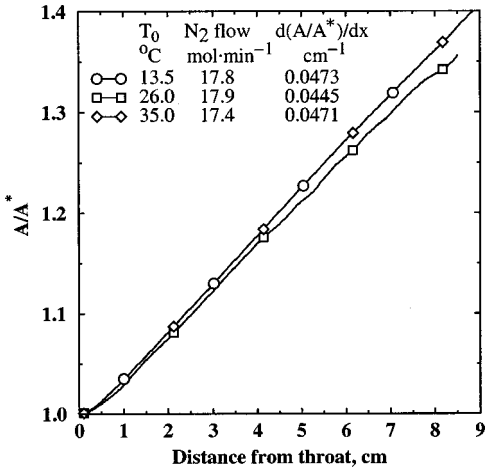

FIG. 2. The effective area ratios and the molar flowrates through the nozzle, for the three sets of condensation experiments, are compared. The nozzle was reassembled before the $T_0=26\,^{\circ}\mathrm{C}$ experiments and this changed both the expansion rates and the region over which the expansion is linear. The symbols correspond to every tenth data point.

Additional changes to the experimental apparatus had little effect on the flow. For example, in the experiments starting from $T_0=26.0\,^{\circ}\mathrm{C}$, the nozzle blocks, shown in Fig. 1, were slightly modified by adding an extra o-ring to minimize leakage through the screw holes. For an unglued nozzle with sidewalls containing windows, typical leakage rates were ~0.004 mol/min, or less than 0.03% of the total flow rate through the nozzle. This is an upper bound on the leakage rates for the $T_0=13.5$ and $35.0\,^{\circ}\mathrm{C}$ experiments where solid sidewalls were used. The leakage rates for the experiments starting from $T_0=26.0\,^{\circ}\mathrm{C}$, including the SANS experiments, were also reduced because the nozzle was glued together. Finally, for the $26.0\,^{\circ}\mathrm{C}$ experiments, we used both a new flow straightener with the RTD probe shifted slightly off center to reduce contact with the pressure probe, and a new flange between the nozzle and the flow straightener that reduced the nonisentropic pressure losses to 0.33 kPa.

Although we would prefer to assemble a nozzle only

TABLE I. The physical properties of H_2O, D_2O, and N_2 required to evaluate the pressure traces. M is the molecular weight (Ref. 26 for N_2), p_v is the equilibrium vapor pressure (Ref. 27 for H_2O and Ref. 28 for D_2O), C_p is the constant pressure heat capacity of the gas, and C_{pl} is the constant pressure heat capacity for the liquid. The heats of vaporization are derived from the equilibrium vapor pressure curves using the Clausius–Clapeyron equation. Unreferenced data are from Lange.[a]

H_2O
$M=18.02\ \mathrm{g\,mol^{-1}}$
$p_v(\mathrm{Pa})=\exp(77.344\,91-7\,235.424\,65/T-8.2\ln T+0.005\,711\,3T)$
$C_p(T=298.15\ \mathrm{K})=33.60\ \mathrm{J\,mol^{-1}\,K^{-1}}$
$C_{pl}(T=273.15\ \mathrm{K})=75.99\ \mathrm{J\,mol^{-1}\,K^{-1}}$
D_2O
$M=20.03\ \mathrm{g\,mol^{-1}}$
$p_v=p_c\cdot\exp[T_c/T(A_1\tau+A_2\tau^{1.9}+A_3\tau^2+A_4\tau^{5.5}+A_5\tau^{10})]$
$p_c=21.66\times10^6$ Pa
$T_c=643.89$ K
$\tau=1-T/T_c$
$A_1=-7.815\,83$
$A_2=17.6012$
$A_3=-18.1747$
$A_4=-3.924\,88$
$A_5=4.191\,74$
$C_p(T=298.15\ \mathrm{K})=34.25\ \mathrm{J\,mol^{-1}\,K^{-1}}$
$C_{pl}(T=293.14\ \mathrm{K})=84.23\ \mathrm{J\,mol^{-1}\,K^{-1}}$
N_2
$M=28.013\ \mathrm{g\,mol^{-1}}$
$C_p(T=298.15\ \mathrm{K})=29.124\ \mathrm{J\,mol^{-1}\,K^{-1}}$

[a]See Ref. 29.

TABLE II. H_2O–D_2O onset conditions for expansions starting from a stagnation temperature of $T_0=13.5\,^{\circ}\mathrm{C}$. The stagnation pressure is p_0, the partial pressures of H_2O and D_2O are p_1 and p_2, respectively, p/p_0 is the expansion ratio at onset, and T is the temperature at onset.

Stagnation ($T_0=13.5\pm0.1\,^{\circ}\mathrm{C}$)				Onset			
p_0 (kPa)	T_0 (°C)	p_1 (Pa)	p_2 (Pa)	p/p_0	p_1 (Pa)	p_2 (Pa)	T (K)
100 mol % H_2O							
59.65	13.50	437.2	⋯	0.3557	155.5	⋯	213.7
59.61	13.50	369.2	⋯	0.3406	125.8	⋯	211.1
59.67	13.50	309.8	⋯	0.3217	99.7	⋯	207.7
59.53	13.49	251.7	⋯	0.3038	76.5	⋯	204.3
59.59	13.49	199.5	⋯	0.2869	57.2	⋯	201.0
59.59	13.49	155.1	⋯	0.2642	41.0	⋯	196.4
59.69	13.52	114.5	⋯	0.2366	27.1	⋯	190.3
20 mol % D_2O							
59.68	13.51	347.0	86.7	0.3625	125.8	31.4	214.9
59.68	13.50	252.5	63.1	0.3309	83.6	20.9	209.4
59.68	13.49	205.2	51.3	0.3077	63.1	15.8	205.1
59.66	13.50	158.1	39.5	0.2889	45.7	11.4	201.4
59.65	13.50	125.8	31.4	0.2676	33.7	8.4	197.1
59.65	13.50	94.3	23.6	0.2431	22.9	5.7	191.8
40 mol % D_2O							
59.66	13.50	259.4	173.1	0.3648	94.6	63.1	215.3
59.61	13.49	224.1	149.5	0.3514	78.8	52.5	213.0
59.60	13.49	188.5	125.8	0.3344	63.1	42.1	210.0
59.63	13.50	153.4	102.3	0.3135	48.1	32.1	206.2
59.62	13.49	118.3	78.9	0.2908	34.4	22.9	201.8
59.61	13.50	94.0	62.7	0.2737	25.7	17.2	198.4
59.62	13.48	70.9	47.3	0.2540	18.0	12.0	194.2
60 mol % D_2O							
59.69	13.50	172.5	259.0	0.3726	64.3	96.5	216.6
59.65	13.49	149.0	223.8	0.3592	53.5	80.4	214.3
59.62	13.50	125.5	188.5	0.3422	42.9	64.5	211.4
59.61	13.51	101.8	152.8	0.3197	32.5	48.9	207.3
59.59	13.49	77.2	116.0	0.2969	22.9	34.4	203.0
59.62	13.48	62.5	93.9	0.2784	17.4	26.1	199.3
59.58	13.50	47.0	70.6	0.2500	11.7	17.6	193.3
80 mol % D_2O							
59.63	13.49	85.9	343.4	0.3780	32.5	129.8	217.5
59.63	13.50	74.3	296.9	0.3643	27.1	108.2	215.2
59.56	13.50	62.5	249.7	0.3492	21.8	87.2	212.6
59.68	13.50	50.7	202.6	0.3270	16.6	66.3	208.7
59.63	13.49	39.0	156.2	0.3025	11.8	47.2	204.1
59.60	13.49	37.7	151.1	0.3019	11.4	45.6	204.0
59.64	13.49	33.5	134.3	0.2899	9.7	38.9	201.6
59.47	13.51	31.1	124.5	0.2787	8.7	34.7	199.4
59.65	13.49	29.5	118.4	0.2839	8.4	33.6	200.4
59.65	13.49	27.3	109.5	0.2764	7.5	30.3	198.9
59.67	13.49	25.2	101.1	0.2653	6.7	26.8	196.6
100 mol % D_2O							
59.68	13.50	⋯	427.0	0.3837	⋯	163.8	218.4
59.67	13.50	⋯	370.5	0.3669	⋯	135.9	215.6
59.71	13.49	⋯	311.3	0.3512	⋯	109.3	212.9
59.67	13.49	⋯	252.2	0.3297	⋯	83.1	209.2
59.71	13.49	⋯	193.4	0.3062	⋯	59.2	204.8
59.60	13.50	⋯	155.4	0.2867	⋯	44.5	201.0
59.71	13.50	⋯	116.2	0.2595	⋯	30.2	195.3

once, during these experiments we disassembled the nozzle to clean the internal surfaces, in particular the Si windows. Unfortunately, reassembling the nozzle can change both the expansion rate and the area of the throat A^*. Figure 2 illustrates the area ratios obtained for two of the nozzle assemblies, and in the linear part of the expansion the slope changed by about 5%. Small changes in A^* are addressed by measuring the molar flow rate of nitrogen through the nozzle at fixed p_0 and T_0, and these values are included in the legend of Fig. 2. For a given gas mixture at fixed p_0, the molar flow rate through the nozzle varies inversely with the square root of the temperature, hence the molar flow rate for the $T_0=35\,^\circ$C calibration is lower than that for the $T_0=13.5\,^\circ$C calibration even though the geometry is unchanged.

To determine whether the onset conditions depend systematically on the value of T_0, we conducted a final series of D_2O condensation experiments using a single nozzle geometry and a probe ($d_{\text{probe}}=0.90$ mm) that only obstructs about 1% of the nominal throat area. These probes were also supported at the exit of the nozzle by a wire mesh. The presence of this mesh influences the flow field near the nozzle exit and, thus, the final ~0.5 cm of the nozzle was unusable for onset measurements.

B. Data analysis

The onset conditions are derived from the pressure measurements using our established onset criteria of a 0.5 K temperature difference between the condensing flow and an isentropic expansion of the same gas mixture.[2] For the H_2O-D_2O experiments, we are interested in following the phase change beyond onset and, thus, we evaluate the other flow parameters using the more rigorous treatment of the diabatic equations, i.e., Eqs. (10)–(12), and (17) of Ref. 2. The latent heat was evaluated as a function of temperature, and for the mixtures we used molar average values based on the composition of the condensible material entering the system. The physical properties[26–29] used in the data evaluation program are summarized in Table I.

The supercooled vapor in the nozzle is metastable with respect to both the liquid and solid phases. We assume that the aerosol formed consists of liquid droplets because the free energy required to form a liquid interface is lower than the corresponding crystalline interface.[30] Given enough time, the drops should eventually freeze, and two stage phase transitions from supercooled vapor to ice have been observed during nucleation and growth measurements of water made at similar or lower expansion rates.[12,31] If, on the other hand, the temperature of the liquid droplets decreases fast enough to a low enough value, in hypersonic nozzle expansions for example,[32] the diffusion of the liquid water can be slowed to the point that crystallization is suppressed and a viscous, glass-like state forms. We believe that the droplets in our nozzle experiments remain liquid because their small size and the short residence time in the nozzle ($<200\ \mu$s) reduces the probability of ice formation within the drop. If ice were to form, our values derived for the amount of material condensed would be ~10% lower.

If all of the vapor entering the nozzle condensed, the average composition of the droplets would be well defined and would equal the initial vapor composition. Unfortunately, the vapor does not condense completely in any of our experiments over a wide range of T_0 and p_0. The strong chemical similarity between H_2O and D_2O, however, makes it reasonable to treat the condensing mixture as a single compound with properties that are the molar average of the pure component values. In particular, the heats of vaporization differ by less than 7% and thus neither onset nor the final value of the condensate mass fraction g are greatly affected. On the other hand, the droplet composition is most critical for interpreting the SANS data because the intensity of the scattering signal depends both on the aerosol number density and the droplet composition.

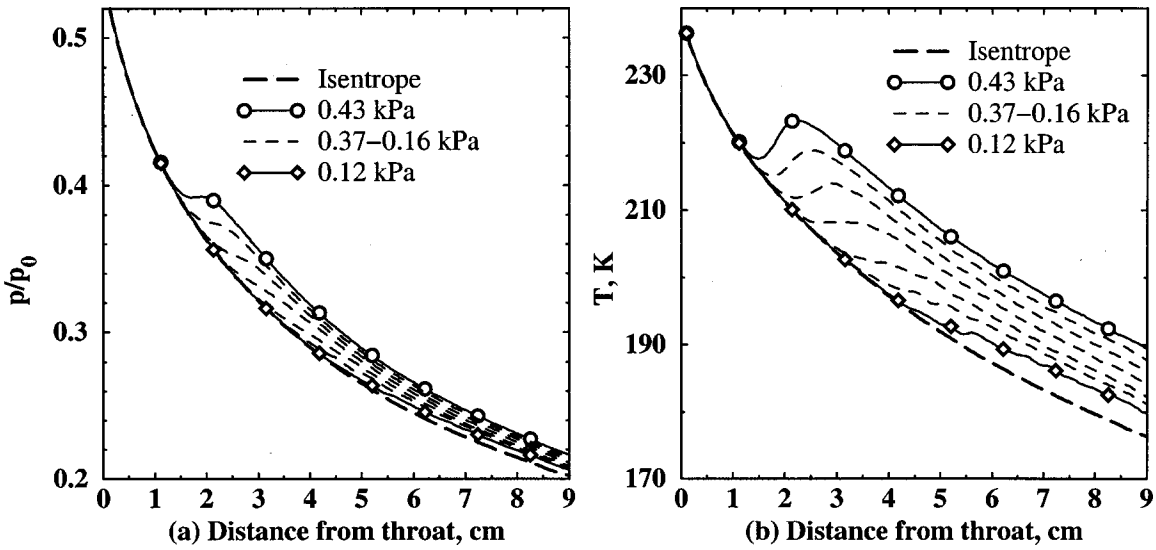

FIG. 3. (a) The measured pressure profiles normalized by the corresponding stagnation pressures (nominally 59.6 kPa) and (b) the derived temperature profiles for the expansion of D_2O and nitrogen starting from $T_0=13.5\,^\circ$C. The open symbols are shown for every tenth data point on the pure component curves only.

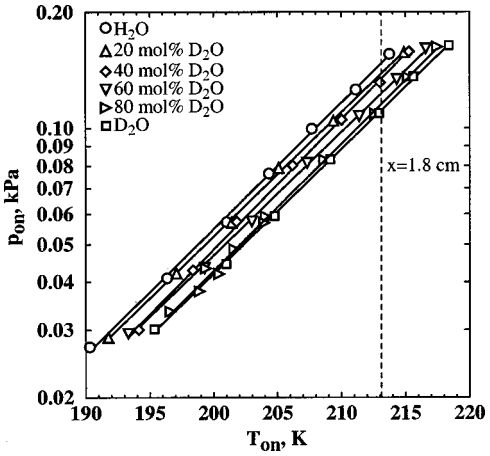

FIG. 4. The onset pressure versus onset temperature for the H_2O-D_2O condensation experiments starting from $T_0=13.5\,^{\circ}C$. The dashed vertical line at 213.1 K ($-60\,^{\circ}C$) corresponds to onset located 1.8 cm downstream of the nozzle throat. Each symbol corresponds to one pressure trace experiment.

Another issue that arises when working with H_2O-D_2O mixtures is that H and D exchange rapidly in both the gas and liquid phase to form HDO. The reaction[33,34]

$$H_2O+D_2O \Leftrightarrow 2\cdot HDO,$$

has an equilibrium constant K given by

$$K=\frac{[HDO]^2}{[H_2O][D_2O]}=3.4-4.0 \quad \text{at} \quad T_0=25\,^{\circ}C.$$

All the liquid mixtures used in the condensation experiments were prepared 0.5 min to 48 h before being used, and were consumed within several hours. Thus, the mixtures should all have had time to equilibrate and in many cases HDO is an important gas phase species. If we assume that HDO has properties that are intermediate to those of H_2O and D_2O, the final mixture will still have properties that are a molar average of those of the pure components.

C. Materials

The D_2O used for these experiments was purchased from Sigma-Aldrich and had more than 99.9% deuterium substitution of the normal hydrogen atoms. The de-ionized H_2O used for these experiments had resistivity values >15 $M\Omega$ cm.

III. RESULTS AND DISCUSSION

The experimental results are presented in the order that they were generated. Thus, we first discuss the condensation experiments starting from 13.5 °C, followed by those starting from 35.0 and 26.0 °C, respectively. We then present an additional series of D_2O experiments conducted using a single nozzle geometry and starting from the three stagnation temperatures.

A. Binary experiments

We conducted 45 condensation experiments for expansions starting from $T_0=13.5\,^{\circ}C$, and Table II summarizes the initial conditions and the conditions at onset. These experiments were our first for this multicomponent system and include the lowest H_2O-D_2O flows. The pressure traces for the pure D_2O experiments and the corresponding temperatures are shown in Fig. 3. The results in Fig. 3 are representative of those observed for H_2O and the intermediate mixtures at all values of T_0.

Figure 4 summarizes the onset values for all of the $T_0=13.5\,^{\circ}C$ experiments on a log p versus T plot (Wilson plot). The circles correspond to the data points for pure H_2O, while the squares are those for pure D_2O. At a given onset tem-

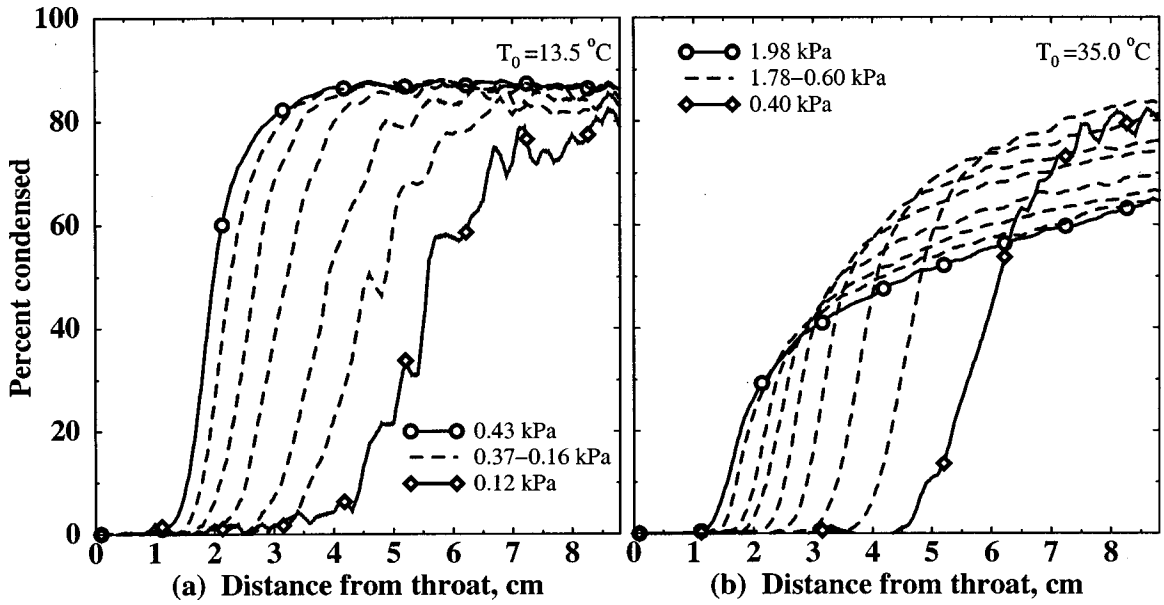

FIG. 5. The percentage of the initial D_2O that condenses in the nozzle is shown as a function of position for expansions starting from: (a) $T_0=13.5\,^{\circ}C$ and (b) $T_0=35.0\,^{\circ}C$. The open symbols are shown for every tenth data point on the pure component curves only. Although a higher percentage of the D_2O vapor entering the nozzle condenses during the $T_0=13.5\,^{\circ}C$ experiments, the absolute amount of condensate (kg condensate/kg flow) increases monotonically with the initial condensible partial pressure.

TABLE III. H_2O-D_2O onset conditions for expansions starting from a stagnation temperature of $T_0=35.0\,°C$. The stagnation pressure is p_0, the partial pressures of H_2O and D_2O are p_1 and p_2, respectively, p/p_0 is the expansion ratio at onset, and T is the temperature at onset.

Stagnation ($T_0=35.0\pm0.1\,°C$)				Onset			
p_0 (kPa)	T_0 (°C)	p_1 (Pa)	p_2 (Pa)	p/p_0	p_1 (Pa)	p_2 (Pa)	T (K)
100 mol % H_2O							
59.63	35.03	2001.3	···	0.3709	742.4	···	232.8
59.64	35.03	1803.7	···	0.3586	646.8	···	230.6
59.57	35.03	1602.4	···	0.3464	555.1	···	228.3
59.64	35.02	1400.9	···	0.3340	467.9	···	225.9
59.57	35.04	1203.0	···	0.3169	381.2	···	222.5
59.67	35.02	1003.2	···	0.3007	301.7	···	219.2
59.65	35.01	802.8	···	0.2837	227.8	···	215.5
59.67	35.01	603.0	···	0.2604	157.1	···	210.3
59.60	35.02	400.8	···	0.2376	95.2	···	204.9
59.56	35.03	200.7	···	0.1901	38.2	···	192.2
20 mol % D_2O							
59.69	35.01	1613.9	403.3	0.3762	607.2	151.7	233.7
59.70	35.01	1287.8	322.2	0.3571	459.9	115.1	230.2
59.67	35.02	968.6	242.5	0.3234	313.3	78.4	223.8
59.62	35.02	810.1	202.5	0.1907	154.5	38.6	192.9
59.70	35.02	646.9	162.0	0.2857	184.8	46.3	216.0
59.62	35.01	486.7	121.6	0.2657	129.3	32.3	211.5
59.66	35.00	322.5	80.8	0.2391	77.1	19.3	205.2
40 mol % D_2O							
59.67	35.02	1220.2	814.1	0.3968	484.2	323.0	237.3
59.65	35.02	974.5	649.1	0.3555	346.4	230.7	229.9
59.57	35.02	732.8	488.7	0.3302	242.0	161.4	225.1
59.66	35.02	609.0	405.6	0.3126	190.3	126.8	221.6
59.61	35.02	488.2	325.7	0.2955	144.3	96.3	218.1
59.65	35.03	357.3	238.3	0.2704	96.6	64.4	212.6
59.63	35.02	243.4	162.1	0.2461	59.9	39.9	206.9
60 mol % D_2O							
59.69	35.03	816.0	1226.2	0.3865	315.4	474.0	235.6
59.68	35.02	655.9	985.2	0.3635	238.5	358.2	231.4
59.67	35.03	492.1	737.8	0.3353	165.0	247.4	226.1
59.67	35.01	408.7	613.9	0.3159	129.1	193.9	222.3
59.66	35.01	327.8	491.5	0.2989	98.0	146.9	218.8
59.66	35.00	246.9	370.9	0.2767	68.3	102.6	214.0
59.62	35.02	164.1	246.5	0.2529	41.5	62.3	208.6
80 mol % D_2O							
59.69	35.03	411.2	1645.1	0.3984	163.8	655.4	237.6
59.67	35.02	330.1	1321.2	0.3722	122.9	491.8	233.0
59.65	35.01	244.1	976.0	0.3397	82.9	331.5	226.9
59.61	35.01	206.6	827.2	0.3233	66.8	267.4	223.7
59.64	35.02	164.8	658.9	0.3030	49.9	199.7	219.6
59.65	35.01	124.3	497.1	0.2819	35.0	140.1	215.1
59.65	35.00	82.7	331.2	0.2562	21.2	84.9	209.3
100 mol % D_2O							
59.62	35.04	···	1982.3	0.3969	···	786.7	237.3
59.53	35.02	···	1783.4	0.3852	···	686.9	235.3
59.62	35.02	···	1589.1	0.3656	···	580.9	231.8
59.64	35.02	···	1392.0	0.3540	···	492.8	229.7
59.62	35.01	···	1184.4	0.3381	···	400.4	226.6
59.59	35.02	···	989.6	0.3222	···	318.9	223.5
59.65	35.01	···	795.9	0.3031	···	241.3	219.7
59.63	35.02	···	597.9	0.2799	···	167.4	214.7
59.58	35.02	···	401.4	0.2552	···	102.5	209.1
59.61	35.03	···	199.9	0.2071	···	41.4	197.0

perature, the higher onset pressure for H_2O primarily reflects the higher equilibrium vapor pressure of H_2O. Because the H_2O onset pressures are only about 30% higher than those for D_2O, individual onset data points for adjoining compositions occasionally overlap. Nevertheless, the data in Fig. 4 show that the onset pressures decrease uniformly as the relative D_2O content of the condensible vapor increases. As in the earlier water-n-alcohol experiments,[2] the onset pressures for a fixed ratio of condensible vapors are exponential functions of temperature and the fit lines are reasonably parallel. The results illustrated in Fig. 4 are representative of the Wilson plots for the experiments starting at higher T_0.

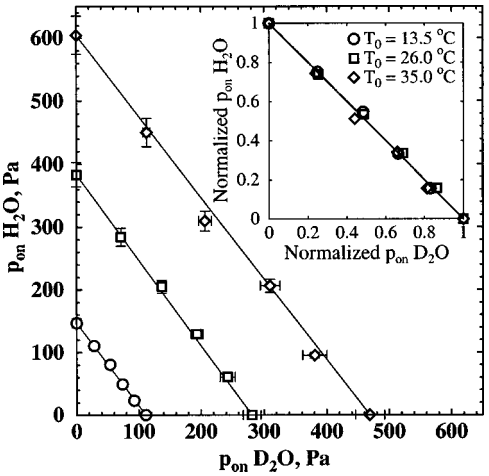

FIG. 6. The H_2O-D_2O onset pressures required to maintain onset 1.8 cm downstream of the throat. The onset temperatures corresponding to the stagnation temperatures of 13.5, 26.0, and 35.0 °C are 213.1, 223.7, and 229.3 K, respectively. In the inset each curve has been normalized by the corresponding onset pressures of the pure components.

Figure 5(a) illustrates the extent of condensation observed for all of the pure D_2O experiments starting from $T_0=13.5\,°C$. As the condensible pressure decreases, the phase change starts further downstream of the throat and becomes less abrupt. For the experiments starting at $T_0=13.5\,°C$, roughly 87% of the initial vapor condensed for all but the lowest condensible vapor concentrations.

We conducted 48 condensation experiments starting from $T_0=35.0\,°C$, and Table III summarizes the results. Although these experiments had the highest condensible partial pressures, the inital concentration of condensible in the gas stream was always <3.5 mol % and, thus, the isentropic portion of the expansion still matched that of pure N_2. In the Wilson plot (not shown) the onset pressures again decreased in a systematic and uniform manner as the condensible vapor became richer in D_2O. Figure 5(b) illustrates that at these vapor concentrations, the condensation process is markedly different than that observed for the low temperature experiments. In particular, at the nozzle exit the experiments do not all reach the same degree of condensation. Instead we see that as the initial condensible vapor concentration increases, the fraction of incoming vapor that condenses systematically decreases. Indeed, at the highest partial pressure of the condensible vapor, only ~60% of the incoming material condenses by the nozzle exit, and, furthermore, significant condensation is still taking place. The pure D_2O results, shown in Fig. 5(b), are again representative of those for pure H_2O and the mixtures. This trend makes sense physically, because in the limit of steam condensation, Moses and Stein[7] ob-

TABLE IV. H_2O–D_2O onset conditions for expansions starting from a stagnation temperature of $T_0 = 26.0\,°C$. The stagnation pressure is p_0, the partial pressures of H_2O and D_2O are p_1 and p_2, respectively, p/p_0 is the expansion ratio at onset, and T is the temperature at onset.

Stagnation ($T_0 = 26.0 \pm 0.1\,°C$)				Onset				Stagnation ($T_0 = 26.0 \pm 0.1\,°C$)				Onset			
p_0 (kPa)	T_0 (°C)	p_1 (Pa)	p_2 (Pa)	p/p_0	p_1 (Pa)	p_2 (Pa)	T (K)	p_0 (kPa)	T_0 (°C)	p_1 (Pa)	p_2 (Pa)	p/p_0	p_1 (Pa)	p_2 (Pa)	T (K)
100 mol % H_2O								60 mol % D_2O							
59.62	25.99	1501.3	⋯	0.3978	597.2	⋯	230.4	59.53	25.99	503.2	754.9	0.3991	200.8	301.2	230.6
59.66	26.00	1467.7	⋯	0.3885	570.2	⋯	228.9	59.59	26.01	467.1	700.7	0.3876	181.1	271.6	228.7
59.64	26.01	1225.9	⋯	0.3740	458.5	⋯	226.4	59.58	26.00	431.1	646.8	0.3769	162.5	243.8	226.9
59.63	26.02	1049.4	⋯	0.3585	376.2	⋯	223.7	59.59	26.01	360.2	540.3	0.3568	128.5	192.8	223.3
59.61	25.99	876.9	⋯	0.3379	296.3	⋯	219.9	59.65	26.01	288.0	432.0	0.3334	96.0	144.1	219.1
59.63	26.00	701.0	⋯	0.3136	219.8	⋯	215.3	59.62	26.00	252.0	378.0	0.3197	80.6	120.9	216.5
59.50	26.00	623.0	⋯	0.3075	191.6	⋯	214.1	59.56	26.00	215.8	323.8	0.3090	66.7	100.1	214.3
59.55	26.01	464.8	⋯	0.2788	129.6	⋯	208.2	59.65	26.01	180.3	270.5	0.2934	52.9	79.4	211.2
59.54	26.01	409.2	⋯	0.2704	110.7	⋯	206.3	59.64	26.00	143.6	215.5	0.2700	38.8	58.2	206.2
59.64	26.01	356.3	⋯	0.2606	92.9	⋯	204.2	59.60	26.00	122.0	183.0	0.2634	32.1	48.2	204.8
59.59	26.00	321.5	⋯	0.2534	81.5	⋯	202.6	59.55	26.00	108.3	162.5	0.2547	27.6	41.4	202.8
59.57	26.01	287.0	⋯	0.2469	70.8	⋯	201.0								
20 mol % D_2O								80 mol % D_2O							
59.65	26.01	1029.9	257.5	0.3895	401.1	100.3	229.0	59.63	26.02	250.9	1001.1	0.4068	102.1	407.2	231.9
59.60	26.00	957.2	239.4	0.3787	362.5	90.6	227.2	59.67	26.02	241.2	962.4	0.4031	97.2	387.9	231.3
59.62	26.00	881.1	220.3	0.3700	326.0	81.5	225.7	59.52	26.03	221.9	885.5	0.3862	85.7	342.0	228.5
59.59	26.00	733.9	183.5	0.3519	258.2	64.6	222.5	59.55	26.00	184.8	737.2	0.3654	67.5	269.3	224.9
59.59	26.00	590.0	147.5	0.3291	194.2	48.6	218.2	59.56	26.00	148.2	591.2	0.3441	51.0	203.4	221.0
59.55	25.99	514.9	128.7	0.3134	161.4	40.3	215.2	59.59	26.00	129.6	517.0	0.3243	42.0	167.7	217.3
59.53	26.02	442.9	110.7	0.2999	132.8	33.2	212.6	59.63	26.02	111.3	444.3	0.3145	35.0	139.7	215.4
59.63	25.99	368.7	92.2	0.2824	104.1	26.0	208.9	59.59	25.99	93.0	371.0	0.2951	27.4	109.5	211.5
59.59	26.02	295.0	73.8	0.2685	79.2	19.8	205.9	59.65	26.01	74.0	295.4	0.2785	20.6	82.3	208.1
59.63	26.00	251.8	63.0	0.2558	64.4	16.1	203.1	59.62	26.00	63.1	251.6	0.2672	16.9	67.2	205.6
59.62	25.99	206.8	51.7	0.2403	49.7	12.4	199.5	59.63	26.00	52.1	208.1	0.2521	13.1	52.5	202.2
40 mol % D_2O								100 mol % D_2O							
59.55	26.01	764.6	509.7	0.3904	298.5	199.0	229.2	59.61	26.01	⋯	1217.7	0.4081	⋯	497.0	232.1
59.64	26.01	708.6	472.3	0.3834	271.7	181.1	228.0	59.64	26.01	⋯	1132.3	0.4042	⋯	457.6	231.4
59.63	26.00	654.5	436.3	0.3750	245.4	163.6	226.5	59.61	26.00	⋯	1038.7	0.3891	⋯	404.2	228.9
59.60	26.00	544.3	362.8	0.3523	191.7	127.8	222.5	59.57	26.01	⋯	874.4	0.3686	⋯	322.3	225.4
59.64	26.01	436.8	291.1	0.3295	143.9	95.9	218.3	59.53	25.99	⋯	782.7	0.3564	⋯	279.0	223.3
59.61	26.00	381.7	254.4	0.3161	120.6	80.4	215.7	59.56	26.01	⋯	654.0	0.3381	⋯	221.1	219.9
59.60	26.01	327.7	218.4	0.3053	100.1	66.7	213.6	59.62	26.00	⋯	561.7	0.3228	⋯	181.3	217.0
59.62	26.02	272.8	181.8	0.2868	78.2	52.1	209.8	59.54	26.02	⋯	504.1	0.3135	⋯	158.1	215.2
59.63	25.99	216.7	144.5	0.2689	58.3	38.9	206.0	59.64	26.01	⋯	411.8	0.2969	⋯	122.3	211.9
59.54	26.00	184.5	123.0	0.2562	47.3	31.5	203.2	59.64	25.99	⋯	351.6	0.2790	⋯	98.1	208.2
59.53	26.00	152.7	101.8	0.2488	38.0	25.3	201.5	59.56	26.00	⋯	321.9	0.2708	⋯	87.1	206.4
								59.63	26.01	⋯	287.7	0.2651	⋯	76.3	205.2
								59.56	26.01	⋯	268.5	0.2584	⋯	69.4	203.7
								59.61	26.00	⋯	251.5	0.2557	⋯	64.3	203.1

served that only about 5% of the steam had condensed by the exit of their nozzle.

We conducted 70 condensation experiments for expansions starting from $T_0 = 26.0\,°C$, and Table IV summarizes the results. Even though the nozzle geometry was slightly different for these experiments, the data are consistent with the results starting from $T_0 = 13.5$ and $35\,°C$.

In our nozzles, the most reliable data are those where onset is not too close to the throat or the end of the nozzle. This region corresponds roughly to that part of the nozzle where the area ratio increases linearly, and generally extends from 1.5 to 7 cm downstream of the throat. We therefore examined the change in onset behavior as a function of H_2O–D_2O ratio in this region. In Fig. 4, the vertical dashed line at 213.1 K($\sim -60\,°C$) corresponds to a position in the nozzle that is 1.8 cm downstream of the throat. We obtained the total onset pressures at this temperature from the exponential fits corresponding to each of the condensible vapor compositions. We calculated the partial pressures of H_2O and D_2O assuming that the ratio of H_2O:D_2O in the gas phase was that of the initial gas mixture. This assumption is reasonable because very little material has condensed at onset. We also determined the partial pressures of H_2O and D_2O corresponding to an onset 1.8 cm downstream of the throat for the experiments starting at the two higher stagnation temperatures. By comparing our results this way, we ensure that all of the gas mixtures experienced the same expansion rate history prior to onset.

Figure 6 illustrates that for all three values of T_0, the isothermal onset pressures for the mixtures vary linearly between those of pure H_2O and pure D_2O, consistent with the expected ideal liquid mixture behavior. Higher values of T_0 and initial condensible pressure p_{c0} lead, of course, to correspondingly higher values of p_{on} and T_{on}. When the onset

TABLE V. Repeat D_2O onset conditions with one nozzle assembly.

Stagnation conditions				Onset			
p_0 (kPa)	T_0 (°C)	p_1 (Pa)	p_2 (Pa)	p/p_0	p_1 (Pa)	p_2 (Pa)	T (K)
$T_0=13.5\pm0.1$ °C							
59.68	13.49	⋯	482.2	0.3793	⋯	182.9	217.7
59.66	13.50	⋯	344.1	0.3442	⋯	118.5	211.8
59.66	13.50	⋯	389.3	0.3554	⋯	138.3	213.7
59.63	13.50	⋯	229.7	0.3054	⋯	70.1	204.6
59.66	13.49	⋯	137.7	0.2627	⋯	36.2	196.0
59.66	13.49	⋯	182.9	0.2868	⋯	52.4	201.0
$T_0=26.0\pm0.1$ °C							
59.67	26.01	⋯	1080.5	0.3957	⋯	427.5	230.0
59.68	26.01	⋯	1077.2	0.3919	⋯	422.2	229.4
59.69	26.01	⋯	1047.4	0.3897	⋯	408.1	229.0
59.69	26.00	⋯	738.3	0.3565	⋯	263.2	223.3
59.69	25.99	⋯	539.6	0.3291	⋯	177.6	218.2
59.69	26.00	⋯	312.4	0.2862	⋯	89.4	209.7
59.67	26.00	⋯	230.0	0.2528	⋯	58.1	202.4
Insulated $T_0=35.0\pm0.1$ °C							
59.74	35.01	⋯	1454.3	0.3877	⋯	563.8	235.6
59.65	35.02	⋯	1213.0	0.3612	⋯	438.1	230.9
59.80	35.00	⋯	973.7	0.3463	⋯	337.2	228.1
59.75	35.00	⋯	726.0	0.3226	⋯	234.2	223.5
59.69	35.00	⋯	484.9	0.2856	⋯	138.5	215.9
59.73	35.01	⋯	243.8	0.2305	⋯	56.2	203.1
$T_0=35.0\pm0.1$ °C[3]							
59.66	35.00	⋯	1252.7	0.3579	⋯	448.4	230.3
59.69	35.02	⋯	569.4	0.2886	⋯	164.3	216.6

pressure curves in Fig. 6 are normalized with respect to the pure H_2O and D_2O pressures, as shown in the inset of Fig. 6, the three curves collapse onto one. There is a small amount of scatter around the dashed line connecting the normalized pure H_2O and D_2O pressures, due to experimental error, but ideal behavior is clearly indicated for the mixtures. The error bars are derived by assuming a 1 K uncertainty in the value of T_0 and a 5% uncertainty in p_{on}.

B. Experiment uncertainty

Because the binary condensation experiments described above were completed using two different nozzle assemblies, we conducted an additional set of D_2O experiments starting from the three different stagnation temperatures but using a single nozzle assembly. These results are summarized in Table V and include two $T_0=35.0$ °C experiments from Dieregsweiler.[3]

Figure 7 illustrates the D_2O onset pressure curves for these experiments. The curves almost coincide with only a small decrease in the onset pressure for a given onset temperature as T_0 is increased. Alternatively, at a fixed onset pressure, for example $p_{on}=0.1$ kPa, there is 1–2 K difference in the onset temperature for experiments that start from 13.5 °C and those that start from 26 or 35 °C. In contrast, the D_2O data in Tables II–IV show the opposite trend, i.e., at a fixed onset pressure the onset line for the 13.5 °C data lies about ~1–2 K to the right of the 35 °C data. Our concern is that our measurements contain a systematic bias, primarily associated with the position of the RTD probe, and that the measured temperatures were influenced by the ambient room temperature.

We therefore insulated the flow straightener and the portion of the RTD probe exposed to ambient conditions and repeated the 35 °C experiments because these are the furthest from room temperature. The shift between the insulated and

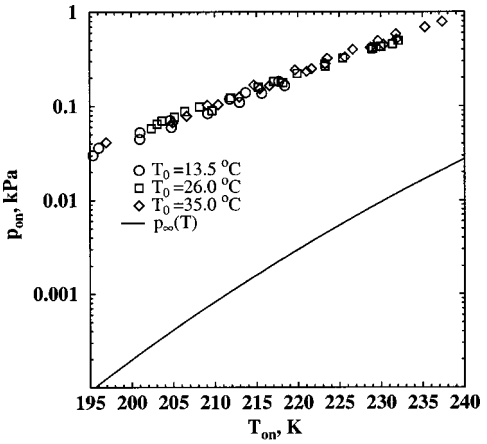

FIG. 8. The D_2O onset measurements are compared to the equilibrium vapor pressure curve (see Ref. 28). On this scale the data overlap quite well.

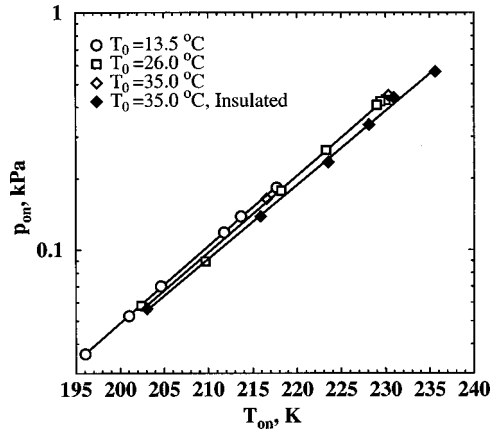

FIG. 7. Some of the variability in the D_2O onset pressures measured using a single nozzle assembly may depend on the degree of insulation on the system.

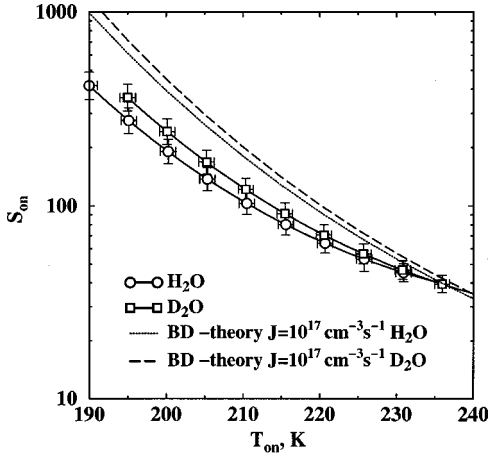

FIG. 9. The supersaturation at onset for D_2O and H_2O increase rapidly as T_{on} decreases. The experimental trend is consistent with the predictions of classical nucleation theory.

uninsulated $T_0 = 35.0\,^{\circ}\mathrm{C}$ data suggest that the temperature measured by the RTD probe reflects both the temperature of the gas entering the nozzle, as well as the temperature of the flow straightener walls and the exposed portion of the probe. The latter approaches room temperature. To obtain a reading of $T_0 = 35.0\,^{\circ}\mathrm{C}$, the gas may have been slightly overheated in the uninsulated experiments and, thus, condensation was shifted slightly downstream to lower temperatures. The degree of overheating for the uninsulated experiments is, however, constrained by the bath temperature and this was $<2\,^{\circ}\mathrm{C}$ warmer than that of the insulated experiments. Since room temperature is $\approx 20\,^{\circ}\mathrm{C}$, this effect is less important for the $T_0 = 26.0$ and $13.5\,^{\circ}\mathrm{C}$ data.

Ideally, the whole system should be in a temperature controlled environment with the ambient temperature close to the stagnation temperature. Currently, the parts of the experimental system containing vapor are insulated. The suspected bias in temperature measurement does not alter the interpretation of the binary data taken at a fixed stagnation temperature. It only changes the temperature difference between the three series of experiments, and even this uncertainty is constrained by the measured values of T_0 and the corresponding water bath temperature. Although we believe this bias exists, we have not corrected the data in Tables II–IV.

C. Critical supersaturation curves for D_2O and H_2O

Figure 8 presents all of the pure D_2O onset pressures and compares them to the equilibrium vapor pressure. On this scale, the data are consistent and define the limit to which D_2O vapor can be supersaturated before condensation occurs in our nozzle. The H_2O data in Tables II–IV define a similar sharp curve, and these data in turn agree with our previously published water measurements.

Homogeneous nucleation is a strong function of both supersaturation and temperature. To examine how the supersaturation at onset varies with T_{on}, we fit all of the onset pressure data for pure D_2O, shown in Fig. 8, to an exponential function of onset temperature and divided this function by the equilibrium vapor pressure. We treated the H_2O onset values presented in Tables II–IV in the same way. Figure 9 shows that the supersaturation at onset for both species increases rapidly with decreasing temperature reaching nearly 400 at the lowest values of T_{on}. Although the Wilson plots all show that the onset pressures for H_2O lie above those for D_2O, once p_{on} is normalized by the equilibrium vapor pressure at T_{on} the supersaturation at onset for H_2O is lower than for D_2O over most of our temperature range. Only as T_{on} approaches 235–240 K do the two curves merge. We note that at these higher temperatures, Wölk and Strey[14] found no difference in the measured nucleation rate between D_2O and H_2O when they plotted their results in terms of supersaturation rather than pressure.

Also included in Fig. 8 are lines corresponding to a nucleation rate $J_{BD} = 10^{17}\ \mathrm{cm}^{-3}\,\mathrm{s}^{-1}$ calculated using the Becker–Döring nucleation rate expression.[35] This value of J is close to the peak nucleation rate predicted by a model for nucleation and droplet growth in the nozzle, when the nucleation rate has been adjusted to match the onset of condensation.[23] At high temperatures the theoretical lines agree quite well with the measured onset values. Furthermore, as the temperature decreases, the theoretical curves separate from each other in a manner similar to the experimental curves. Finally, the rapid deviation of the theoretical curves from the experimental ones simply confirms that the temperature dependence of the classical nucleation theory is too strong, an effect that we discuss in more detail in a separate paper.[36]

IV. SUMMARY AND CONCLUSIONS

We investigated the condensation of H_2O, D_2O, and four intermediate mixtures starting from three stagnation temperatures. In this highly ideal system, the onset pressure at constant onset temperature varies linearly between the values for the pure components. The linear relationship is even more pronounced than in the earlier binary measurements made with ethanol–propanol mixtures.[2]

We also pooled the onset measurements for all of the pure species experiments to determine the supersaturation reached by H_2O and D_2O at onset. At high temperatures, $\sim$240 K, the onset saturations are indistinguishable, but as the temperature decreases D_2O appears to reach higher supersaturations than H_2O. This behavior is in agreement with the predictions of the classical nucleation theory.

ACKNOWLEDGMENTS

This work was supported by the National Science Foundation, under Grants Nos. CHE-0097896, CHE-0089136, INT-0089897, and by the Donors of the Petroleum Research Fund administered by the American Chemical Society. We thank Uta Dieregsweiler and Amjad Khan for their assistance in completing the final D_2O experiments.

[1] R. Strey, Y. Viisanen, and P. E. Wagner, J. Chem. Phys. **103**, 4333 (1995).
[2] B. E. Wyslouzil, C. H. Heath, G. Wilemski, and J. L. Cheung, J. Chem. Phys. **113**, 7317 (2000).
[3] U. M. Dieregsweiler, M. S. thesis, Worcester Polytechnic Institute, Worcester, MA, 2001.
[4] K. Oswatitsch, Z. Angew. Math. Mech. **22**, 1 (1942).
[5] H. L. Jaeger, E. J. Willson, and P. G. Hill, J. Chem. Phys. **51**, 5380 (1969).
[6] B. J. C. Wu, P. P. Wegener, and G. D. Stein, J. Chem. Phys. **68**, 308 (1978).
[7] C. A. Moses and G. D. Stein, J. Fluids Eng. **100**, 311 (1978).
[8] D. Barschdorff, Phys. Fluids **18**, 529 (1975).
[9] G. D. Stein and P. P. Wegener, J. Chem. Phys. **46**, 3685 (1967).
[10] R. Miller, R. J. Anderson, J. L. Kassner, and D. E. Hagen, J. Chem. Phys. **78**, 3204 (1983).
[11] P. E. Wagner and R. Strey, J. Phys. Chem. **85**, 2694 (1981).
[12] Y. Viisanen, R. Strey, and H. Reiss, J. Chem. Phys. **99**, 4680 (1993).
[13] Y. Viisanen, R. Strey, and H. Reiss, J. Chem. Phys. **112**, 8205 (2000).
[14] J. Wölk and R. Strey, J. Phys. Chem. B **105**, 11683 (2001).
[15] F. Peters and B. Paikert, Exp. Fluids **7**, 7748 (1989).
[16] C. C. M. Luijten, K. J. Bosschaart, and M. E. H. van Dongen, J. Chem. Phys. **106**, 8116 (1997).
[17] R. Heist and H. Reiss, J. Chem. Phys. **59**, 865 (1973).
[18] H. Flood and L. Tronstad, Z. Phys. Chem. Abt. A **175**, 347 (1936).
[19] C. F. Lee, in *Condensation in High Speed Flows*, edited by A. A. Pouring (American Society of Mechanical Engineers, New York, 1977), pp. 83–96.
[20] B. E. Wyslouzil, J. L. Cheung, G. Wilemski, and R. Strey, Phys. Rev. Lett. **79**, 431 (1997).

[21] B. E. Wyslouzil, J. L. Cheung, G. Wilemski, R. Strey, and J. Barker, Phys. Rev. E **60**, 4330 (1999).
[22] C. H. Heath, K. Streletzky, J. Wölk, B. E. Wyslouzil, and R. Strey, in *Nucleation and Atmospheric Aerosols 2000: 15th International Conference*, edited by B. N. Hale and M. Kulmula (American Institute of Physics, Melville, NY, 2000), pp. 59–62.
[23] C. H. Heath, K. Streletzky, B. E. Wyslouzil, and G. Wilemski, in *Nucleation and Atmospheric Aerosols 2000: 15th International Conference*, edited by B. N. Hale and M. Kulmula (American Institute of Physics, Melville, NY, 2000), pp. 63–66.
[24] G. Wilemski, Phys. Rev. E **61**, 557 (2000).
[25] G. D. Stein, Ph.D. thesis, Yale University, New Haven, CT, 1967.
[26] W. M. Chase, Jr. *et al.*, *JANAF Thermochemical Tables*, 3rd ed. (American Chemical Society, Washington DC, 1985).
[27] P. E. Wagner, *Aerosol Research III* (University of Vienna, Vienna, Austria, 1981), p. 209.
[28] P. G. Hill and R. D. C. MacMillan, J. Phys. Chem. Ref. Data **9**, 735 (1980).
[29] *Lange's Handbook of Chemistry*, 14th ed., edited by J. A. Dean (McGraw–Hill, New York, 1992).
[30] C. A. Knight, *The Freezing of Supercooled Liquids* (Van Nostrand, Princeton, NJ, 1967).
[31] J. Huang and L. S. Bartell, J. Phys. Chem. **99**, 3924 (1995).
[32] L. S. Bartell and R. A. Machonkin, J. Phys. Chem. **94**, 6468 (1990).
[33] H.-C. Chang, K.-H. Huang, Y.-L. Yeh, and S. H. Lin, Chem. Phys. Lett. **326**, 93 (2000).
[34] F. Libnau, A. Christy, and O. Kvalheim, Appl. Spectrosc. **49**, 1431 (1995).
[35] R. Becker and W. Döring, Ann. Phys. (Paris) **24**, 719 (1935).
[36] J. Wölk, R. Strey, C. H. Heath, and B. E. Wyslouzil, J. Chem. Phys. **117**, 4954 (2002).